Cold Regions Research and Engineering Laboratory

US Army Corps of Engineers®
Engineer Research and Development Center

Investigations into the Ice Crystallization and Freezing Properties of the Antifreeze Protein *Ap*AFP752

Emily Asenath-Smith, Emily C. Jeng, Emma K. Ambrogi, Garrett R. Hoch, and Jason L. Olivier

September 2022

The US Army Engineer Research and Development Center (ERDC) solves the nation's toughest engineering and environmental challenges. ERDC develops innovative solutions in civil and military engineering, geospatial sciences, water resources, and environmental sciences for the Army, the Department of Defense, civilian agencies, and our nation's public good. Find out more at www.erdc.usace.army.mil.

To search for other technical reports published by ERDC, visit the ERDC online library at https://erdclibrary.on.worldcat.org/discovery.

Investigations into the Ice Crystallization and Freezing Properties of the Antifreeze Protein *ApAFP752*

Emily Asenath-Smith, Emily C. Jeng, Emma K. Ambrogi, Garrett R. Hoch, and Jason L. Olivier

US Army Engineer Research and Development Center (ERDC)
Cold Regions Research and Engineering Laboratory (CRREL)
72 Lyme Road
Hanover, NH 03755-1290

Technical Report (TR)

Abstract

Antifreeze proteins (AFPs) allow biological organisms, including insects, fish, and plants, to survive in freezing temperatures. While in solution, AFPs impart cryoprotection by creating a thermal hysteresis (TH), imparting ice recrystallization inhibition (IRI), and providing dynamic ice shaping (DIS). To leverage these ice-modulating effects of AFPs in other scenarios, a range of icing assays were performed with AFPs to investigate how AFPs interact with ice formation when tethered to a surface.

In this work, we studied *Ap*AFP752, an AFP from the beetle *Anatolica polita*, and first investigated whether removing the fusion protein attached during protein expression would result in a difference in freezing behavior. We performed optical microscopy to examine ice-crystal shape, microstructure, and the recrystallization behavior of frozen droplets of AFP solutions. We developed a surface chemistry approach to tether these proteins to glass surfaces and conducted droplet-freezing experiments to probe the interactions of these proteins with ice formed on those surfaces.

In solution, *Ap*AFP752 did not show any DIS or TH, but it did show IRI capabilities. In surface studies, the freezing of AFP droplets on clean glass surfaces showed no dependence on concentration, and the results from freezing water droplets on AFP-decorated surfaces were inconclusive.

Contents

Figures

Preface

1 Introduction

1.1 Background

Biological organisms present many design strategies for developing next-generation advanced materials with unique functionalities. For instance, antifreeze proteins (AFPs), found in biological organisms, including fish, insects, and plants, confer protection from the effects of freezing temperatures. Various applications require the prevention of freezing. In the medical field, for example, robust and versatile cryoprotective materials are needed to ensure the quality of frozen medications and vaccines as well as cells, tissues, and embryos (Chang and Zhao 2021). A seemingly disparate but related example is unmanned aerial vehicles, which need lightweight, low-power ice mitigation solutions (Cao et al. 2018). AFPs present a promising solution to icing problems, but further studies are needed to understand their mechanisms.

In general, AFPs do not prevent ice formation but, rather, modulate ice formation in biological media to protect species from damage caused by the uncontrolled growth of ice. The characteristics that define the effects of AFPs on ice growth are dynamic ice shaping, thermal hysteresis, and ice recrystallization inhibition (Ghalamara et al. 2022).

Dynamic ice shaping (DIS) refers to the irreversible binding of AFPs to specific crystallographic planes of ice, inhibiting further growth of those planes. Ice growth depends on many factors, such as supersaturation and temperature. At standard pressure, ice is mainly in the hexagonal ice crystal (I_h) form, schematically shown in Figure 1. The top facet of the crystal, perpendicular to the *c*-axis, is the basal plane, while the sides of the hexagonal crystal have primary and secondary prism planes. There is also a pyramidal prism plane that is formed by intersections at the *c*-axis and two a_n-axes. As temperature is lowered, a regular ice crystal will grow in all directions, with different rates for each plane. The prism facets tend to grow faster than the basal facets, causing them to be less prevalent in the final crystal shape. As the temperature continues to decrease, the prism planes will eventually start to grow dendrites. AFPs can change the shape of ice crystals, from growing in the hexagonal form to growing in different shapes, depending on the planes to which the AFP has bound. Essentially,

AFPs do not stop the formation of ice but, rather, control its growth (Clarke et al. 2002).

Figure 1. Illustration of the notable crystallographic planes within a hexagonal ice crystal.
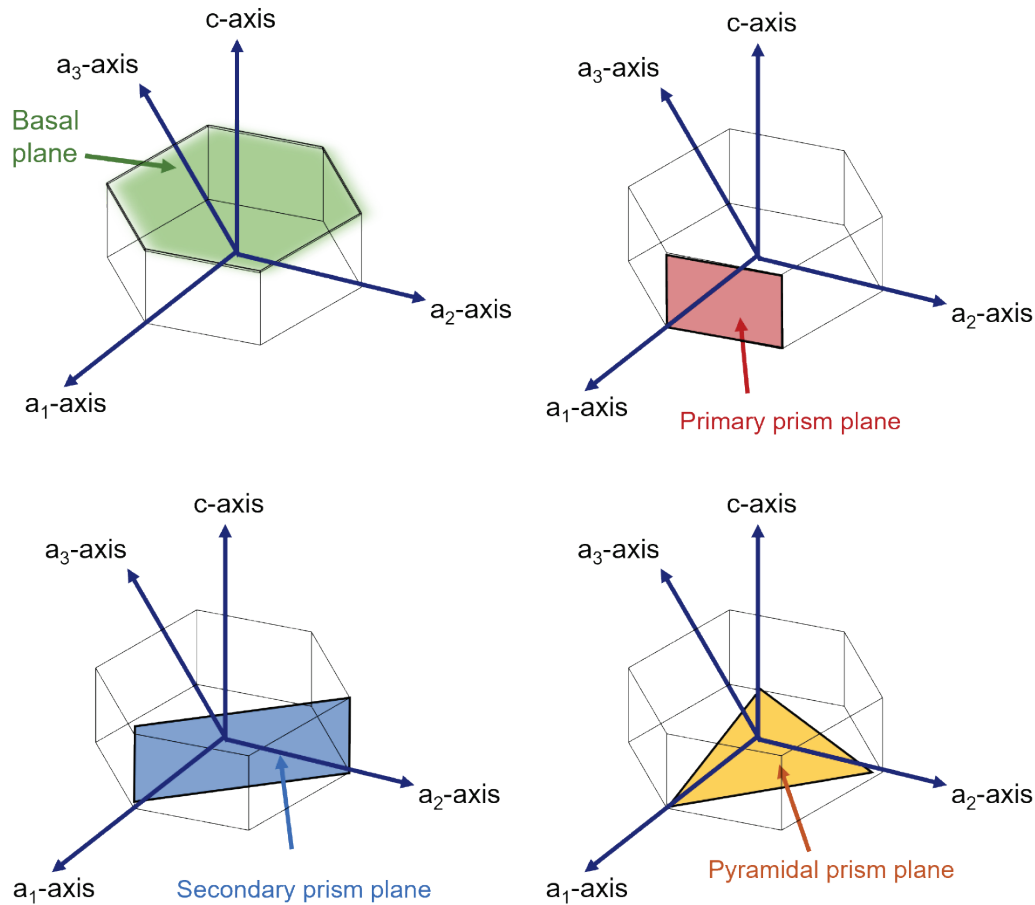
Thermal hysteresis (TH) describes the difference between the freezing temperature and the melting temperature. By shaping the ice, AFPs depress the freezing-point temperature, based on the Gibbs-Thompson effect, which describes how increased surface curvature results in a lowered freezing point (Gerhauser and Gaukel 2021). The TH is a quantitative indication of how strong the activity of the AFP is. At millimolar concentrations, moderate AFPs, which tend to be from fish, have TH values of around 0.5°C to 1.0°C,[*] while hyperactive AFPs, which mainly come from insects, can have TH values of up to 6°C (Celik et al. 2010). The crystallographic planes that AFPs bind to affect the TH; moderate AFPs bind to the

---

prism and pyramidal facets, while hyperactive AFPs bind to the basal facets (Scotter et al. 2006).

Ice recrystallization inhibition (IRI) is the ability to prevent the regrowth of larger ice crystals at the expense of smaller ones while maintaining a constant ice-phase volume. Recrystallization is driven by the Ostwald ripening mechanism, in which water molecules diffuse across the grain boundaries of neighboring ice grains (Budke and Koop 2006); thus, the interfacial energy between the ice grain and the solution is reduced through the regrowth of these larger ice crystals (Budke et al. 2009). AFPs are thought to prevent ice recrystallization through the binding of ice facets; whether this is the only mechanism for IRI is still being debated (Biggs et al. 2019).

In this research, we investigated the properties of *Ap*AFP752. This AFP comes from the beetle *Anatolica polita*, which resides mainly in the Xinjiang and Central Asian regions, where temperatures reach as low as −40°C (Mao et al. 2011). Figure 2*a* shows the structural representation of *Ap*AFP752, which is cysteine-rich and has a beta-helix structure formed by disulfide bonds (Mao et al. 2011). The ice binding surface (IBS) of this AFP is made up of beta sheets consisting of the threonine-cysteine-threonine (TCT) sequence, giving it a flat surface. This sequence follows the TXT motif, where *T* is threonine and *X* is an amino acid, that is seen in the IBSs of other hyperactive insect AFPs, such as the *Tm*AFP (Liou et al. 2000) or sbwAFP (Graether et al. 2000). The threonines of this sequence have hydrophobic methyl groups, responsible for the water molecules rearranging into a clathrate structure, and hydrophilic hydroxyl groups, responsible for anchoring the clathrate arrangement (Garnham et al. 2011). Proteins with such a sequence are expected to be hyperactive due to the match of the spacing between the threonine on the IBS and the distance of the oxygen atoms on the ice planes (Graether et al. 2000; Liou et al. 2000). Previous studies have demonstrated that *Ap*AFP752 does show antifreeze activity, reaching a TH of 0.76°C at 1.0 mg/mL concentrations (Mao et al. 2010). To obtain high concentrations of this AFP, the recombinant protein, TrxA-*Ap*AFP752, must be expressed through *E. coli* (Mao et al. 2011).

Figure 2. (*a*) Structural model of the TrxA-*Ap*AFP752 fusion protein. The circled *magenta arrows* on the *Ap*AFP752 indicate the beta sheets that contain the threonine-cysteine-threonine (TCT) motif, which make up the ice-binding surface. The *blue links* on the *Ap*AFP752 are the disulfide bonds formed through cysteine bonding, forming the beta helix. (Image republished with permission from Mao et al. 2011). (*b*) Structural model of the Type III antifreeze protein (AFP). The *magenta arrows* represent the beta sheets, while the *light blue* sections are the alpha helices. (Image republished from Bialkowska et al. 2020)
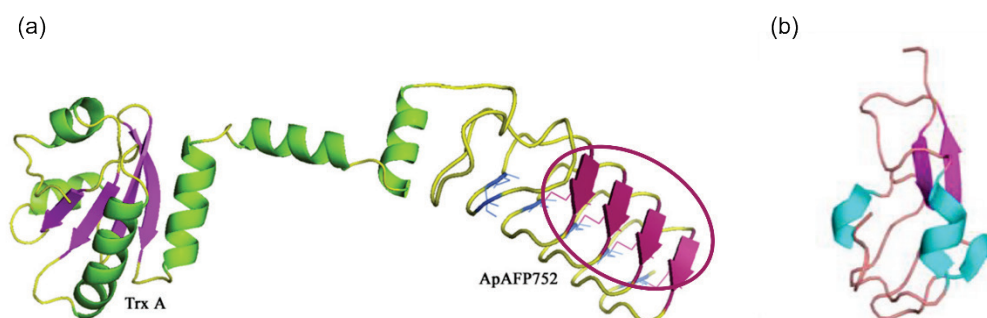
A wild Type III AFP from an eel pout was used as a comparison for results from studies with *Ap*AFP752. This Type III AFP, shown in Figure 2*b*, is a moderate AFP that is globular in shape and consists of a one-turn alpha-helix and beta sheets but does not have any repetitive structural motifs (Chao et al. 1994; Verreault et al. 2018). Unlike other AFPs, the Type III AFP does not have the threonine sequence, and its IBS consists of mostly hydrophobic residues that arrange the water molecules to the IBS (Chakraborty and Jana 2019). The wild Type III AFP is naturally expressed and, therefore, has a mixture of different isoforms: the quaternary aminoethyl (QAE)-Sephadex binding subgroup and the sulfopropyl (SP)-Sephadex binding subgroup, with the QAE isoform responsible for the observable AFP properties, such as DIS and TH (Takamichi et al. 2009).

1.2 Objectives

AFPs have been studied for their ability to prevent ice growth while in an aqueous solution. This has led to their utilization in cryobiology and food science; however, AFPs are not yet developed for applications that require control over ice formation on surfaces. Very little has been studied about how AFPs function when restricted to a two-dimensional platform, such as an aluminum surface (Esser-Kahn et al. 2010; Koshio et al. 2018; Liu et al. 2016; Gwak et al. 2015). We studied the freezing behavior of both the recombinant protein TrxA-*Ap*AFP752, which contains the fusion protein TrxA from expression, and cleaved *Ap*AFP752 in solution form and then pursued studies of surface-grafted AFP752, using a wild Type III AFP as a reference material.

1.3   Approach

First, the antifreeze properties of *Ap*AFP752, such as the ice microstruc-
ture, IRI, TH, and DIS, were studied in solution, along with the Type III
AFP from eelpout for comparison. Next, we conducted freezing experi-
ments for *Ap*AFP752 droplets in oil and on glass surfaces to see if the
AFP's freezing behavior was affected by the presence of a surface. Finally,
we did surface modifications to glass slides via self-assembly to tether
*Ap*AFP752 to glass surfaces and conducted freezing experiments with
those surfaces.

2 Experimental Methods

2.1 Materials

The Trx-*Ap*AFP752, cleaved *Ap*AFP752, and buffer solutions (50 mM KHPO₄, 20 mM NaCl)* were provided by Professor K. Varga (University of New Hampshire, Durham, NH, USA). The provided AFPs were modified with an extra cysteine at the N-terminus or C-terminus of the protein to facilitate surface grafting. Wild Type III AFP was purchased from AF Protein (Waltham, MA, USA).

For surface chemistry experiments, glass slides were obtained from Corning Life Sciences (Tewksbury, MA, USA); silicon wafers were obtained from WaferPro (Santa Clara, CA, USA); N-(6-aminohexyl)aminomethyltriethoxysilane (AHAMTES) was obtained from Gelest (Morrisville, PA, USA); and dimethyl sulfoxide (DMSO), ethylenediamine tetraacetic acid (EDTA), and molecular sieves (Type 3A, 4–8 mesh beads) were obtained from Sigma Aldrich (Burlington, MA, USA). Na₂PO₄ (Acros Organics, 99+%), ethanol (100%), hydrogen peroxide (30%), NaCl (99.0% to 100.5%), and NaOH (99.2%) were obtained from Fisher Scientific (Hampton, NH, USA).

2.2 Antifreeze protein (AFP) and ice microstructure study

Room temperature droplets (10 μL) of AFP solutions were deposited on clean glass slides that were chilled to −16°C in a cold room. Droplets were allowed to freeze under the isothermal conditions of −16°C on the microscope stage. All droplets froze within 5 min. After freezing, droplets were imaged in cross-polarized light with a stereomicroscope (Model SZH-10, Olympus, Bartlett, TN, USA) using a bottom-mounted halogen light source. Images were acquired with a 6-megapixel digital camera (Model Infinity3-6URC, Lumenera, Ottawa, ON, Canada). Images were processed using ImageJ (National Institutes for Health, public domain).

---

* For a full list of the spelled-out forms of the chemical elements used in this document, please refer to *US Government Publishing Office Style Manual*, 31st ed. (Washington, DC: U.S Government Publishing Office, 2016), 265, https://www.govinfo.gov/content/pkg/GPO-STYLEMANUAL-2016/pdf/GPO-STYLEMANUAL-2016.pdf.

## 2.3	Ice recrystallization inhibition (IRI) studies via splat assay

Splat assay experiments, which were conducted to study the IRI ability of AFPs, were modified from previous procedures (Knight et al. 1988). To create a "splat" drop, a dewar of liquid N_2 was placed underneath an aluminum plate. A coverslip was placed on the aluminum plate, which had a local temperature of $-14 \pm 1°C$. A 10 µL droplet of solution was dropped from a height of approximately 1 m onto the coverslip, where it instantly formed a flat ice disk. The coverslip was sealed with vacuum grease and another coverslip on top to prevent evaporation, and the sample was transferred over to a cross-polarizer stage underneath a digital optical microscope (Dino-Lite, Los Angeles, CA, USA), both of which were equilibrated at $-8°C$. Snapshots of the microstructure of the ice were recorded every 30 min. The screenshots after the first 30 min were analyzed using ImageJ to measure 50 of the grains to obtain the mean grain area (MGA).

## 2.4	Dynamic ice shaping (DIS)

The procedure for studying DIS was modeled after previously reported experiments (Drori et al. 2014). A 0.5 µL droplet of solution was deposited in the center of a 22 mm coverslip. The coverslip was sealed with a ring of vacuum grease and another coverslip placed on top to ensure that no sublimation occurred during the testing. The sample was placed on the heating block of a temperature-controlled stage (Model BCS 196, Linkam, Epsom, England, UK), which was placed under a compound microscope (Model BX60, Olympus, Bartlett, TN, USA) and viewed through a 5× objective. Images were acquired with a digital camera (Model GS3-U3-32S4C-C, Teledyne FLIR, Nashua, NH, USA) within the Linkam software (LINK 1.2.17.13) at a rate of 1 image/sec.

Heating and cooling were controlled through the LINK software, with programmed temperature ramps that influenced the pump speed of flowing liquid nitrogen. Initially, the sample was rapidly cooled to $-40°C$ to ensure that the droplet was completely frozen. Then, the sample was heated slowly to as close to the melting point as possible to facilitate the formation of the smallest single crystal possible (target diameter = 10 µm). Due to the sensitivity of the temperature differences affecting the freezing or melting process, the melting point of the buffer was defined as the temperature right before the crystal started refreezing. The temperature was then cooled at a rate of 0.1°C/min or 1°C/min, depending on the rate of melting, to observe the growth of the crystal.

2.5   AFP solution droplet freezing in oil solutions

Droplets (10 µL) of AFP solution were suspended in silicone oil within an aluminum beaker that was placed within an environment chamber with a temperature-controlled Peltier plate. A thermocouple was placed within the oil, adjacent to the suspended droplet. The approximate distance between the droplet and the thermocouple was 1–2 mm. A temperature ramp of 5°C/min was imposed on the plate to heat and cool the system from ambient to −20°C for three cycles. The thermal changes associated with solidification and melting were monitored by the thermocouple, and the freezing temperature was taken as the temperature at the start of the latent heat spike. Five droplets were used for each solution composition, allowing for 15 replicate measurements for each composition.

2.6   Freezing AFP droplets on glass surfaces

Droplet-freezing experiments were carried out in a thermal chamber (Model 9076, Delta Design, Cohu Inc, Poway, CA, USA) equipped with liquid nitrogen for cooling. The heating and cooling of the chamber were controlled with a Python script. The temperature of the droplets was measured with a thermal imaging camera (Model A6703sc, Teledyne FLIR, Nashua, NH, USA) with a 1× microscope lens and 3–5 µm wavelength sensitivity. The 15 µm pixels of the camera provided a resolution of 3×10^{-6} as a proportion of the 9.7 mm × 7.7 mm field of view (640 × 512 pixel array). Integration time (equivalent to shutter speed) was 5 ms. The FLIR software (FLIR Research Studio Professional, 2013) was used to set up the camera parameters and triggering to capture 1 image (frame)/sec.

The camera was calibrated with a blackbody chamber to achieve 0.1°C accuracy from −20°C to 0°C. Emissivity was input manually with a distance-to-target of 0.03 m and the average ambient temperature to convert camera infrared (IR) counts to temperature (Hori et al. 2013). The emissivity of ice crystals and water in the 3–5 µm spectral range were both 0.95–0.98.

A clean glass slide was used as the substrate for the droplets of interest. The glass slide was held in a rectangular insulated foam structure with an open top to minimize evaporation during the experiment. A 10 µL drop of water was placed on the slide, and the IR camera was focused. After closing the chamber, the temperature was equilibrated at 10°C for 10 min, then cooled to −30°C at 1°C/min. The chamber was then ramped back to

10°C at the same rate and cycled, for a second time, down to −30°C. The reported data are from the second freezing cycle.

A temperature of 10°C was chosen as the upper bound because this was the temperature at which the frozen droplet from the first cycle would melt before the second cycle began. Due to air circulation causing minor evaporation, the droplet volume was slightly diminished during the second cycle. A temperature of −30°C was chosen as the lower bound to the ramp program because this resulted in a sample temperature of approximately −20°C, which was cold enough because, even with supercooling, the droplets consistently were frozen before reaching −20°C.

The data were processed in Python (version 3.8.3, Python Software Foundation, public domain) to remove and smooth noise in the data caused by the IR camera recalibrating during the test as a result of the large temperature swings. Plots were created to compare the temperature and length of freezing during the first and second cycle for all concentrations of AFPs as well as for two controls: water and buffer.

2.7 Attaching AFPs to glass surfaces

Prior to functionalization, glass slides and silicon wafers were cleaned by submerging them in freshly prepared Piranha solution (7:3 mixture of sulfuric acid to 30% hydrogen peroxide) for 1 hr (*Caution: Piranha solution reacts violently with organic matter*). After rinsing with water (3×), the slides were dried in an oven at 70°C for 1 hr. Aminosilane functionalization of slides and wafers was carried out in 250 mL anhydrous ethanol under ultrahigh-purity nitrogen to which 2.5 mL AHAMTES was added. The reaction was allowed to proceed at 70°C for 3.5–4 hr. Following the reaction, the slides were rinsed with ethanol (2×) and water (1×), dried in an oven at 70°C for 30 min, and then dried overnight under vacuum.

Three different lengths of succinimide-maleimide polyethylene glycol (SM(PEG)$_n$) crosslinkers were used for the attachment of proteins to glass slides and silicon wafers, where $n = 2$, 12, and 24. The SM(PEG)$_n$ crosslinker stock solutions were prepared by dissolving 100 mg of crosslinker in DMSO to prepare a 250 mM solution—adding 840, 360, or 187 μL DMSO to 100 mg SM(PEG)$_2$, SM(PEG)$_{12}$, and SM(PEG)$_{24}$, respectively. Solutions were then further diluted to 1 mM with DMSO. Crosslinker stock solutions were stored at 5°C.

The SM(PEG)$_n$ crosslinker attachment was performed by submerging AHAMTES-functionalized slides in 45 mL of phosphate-buffered saline (PBS) buffer (pH 7.2) with 1 mM EDTA, to which 45 µL of crosslinker solution was added for a final crosslinker concentration of 0.01 mM. Slides were left in the crosslinker solution for 1 hr, then rinsed with PBS/EDTA buffer and water, and then dried under vacuum for at least 2 hr.

Protein attachment was carried out by submerging crosslinker-functionalized slides in 45 mL of pH 6.0 buffer (50 mM KH$_2$PO$_4$, 20 mM NaCl, adjusted to pH 6.0 with NaOH) for AFP and bovine serum albumin (BSA) or pH 8.0 buffer (150 mM NaCl, 50 mM NaPO$_4$, adjusted to pH 8.0 with NaOH) for Trx-AFP attachment. Protein solutions (100 µM, 22 µL) were added to slides in buffer, and reactions were kept at 4°C overnight (~18 hr). Following reaction, slides were rinsed in buffer and water and then dried under vacuum for at least 2 hr.

2.8 Attaching AFPs to surfaces: surface characterization

The glass surfaces were characterized at each step in the surface-functionalization process. Contact angle goniometry (Model 590, Ramé-Hart, Succasunna, NJ, USA) was used to measure wettability; a Fourier transform infrared (FTIR) spectrometer (Model Nicolete 6700, Thermo Fisher Scientific, Waltham, MA, USA), equipped with a deuterated triglycine sulfate (DTGS) detector and a variable grazing angle attenuated total reflectance accessory (Model VariGATR, Harrick Scientific, Pleasantville, NY, USA), was used to probe for changes in chemical bonds.

2.9 Water-droplet-freezing experiments on surfaces with AFP

Droplet-freezing experiments were carried out in a Delta Design 9076 thermal chamber (Cohu Inc, Poway, CA, USA) equipped with liquid nitrogen for cooling. The heating and cooling of the chamber were controlled with a Python script. An aluminum box was placed inside the chamber to isolate the sample and droplet from winds. Eight thermocouples were placed at various locations in the chamber, both inside and outside the isolation box, so that air, stage surface, and sample temperature could be monitored throughout the experiments. LabVIEW graphical programming environment (National Instruments, Austin, TX, USA) was used to control temperature recordings. Nucleation experiments were recorded with a digital microscope (Model Premier, Dino-Lite, Los Angeles, CA, USA) and a cross-polarized stage using DinoCapture 2.0 software. The frame rate for

all recordings was 10 fps. In all experiments, a substrate was positioned on the stage such that the tip of the thermocouple was in contact with the glass (Figure 3). A 10 µL drop of water was placed on the sample, and the microscope was focused on the drop. The chamber was shut, and video and temperature recordings were begun. The temperature was equili-brated at 10°C for 10 min and then cooled to −30°C at 20°C/min. The chamber was held at −30°C for 10 min, during which time the temperature inside the isolation box decreased and the droplets froze. Then the cham-ber was warmed to ambient temperature, and the sample was removed.

Figure 3. A picture of the experimental set up used for water-droplet-freezing experiments on modified surfaces.
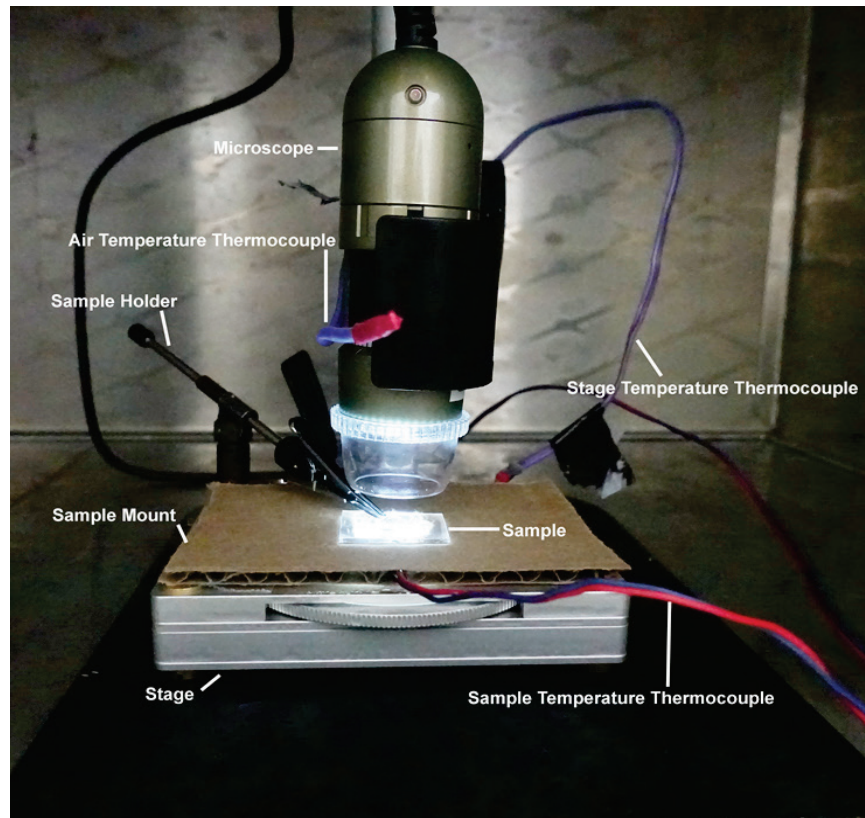
3 Results

3.1 Effect of *Ap*AFP752 on the microstructure of polycrystalline ice

While AFPs are widely known to shape individual ice crystals, their effect on shaping grains within polycrystalline microstructures is not yet understood. Therefore, we investigated the microstructures of polycrystalline ice specimens made by freezing droplets. Because all AFP solutions are stabilized in a buffer, we performed all experiments relative to the buffer alone and to pure water. The individual 10 μL droplets of water all froze within 5 min at −16°C. Imaging of pure-water ice showed the dendritic polycrystalline structure characteristic of isothermally frozen ice (Figure 4*a*), without any preferential crystallographic orientation of the grains, as evidenced by the full spectrum of colors present in cross-polarized light. The ice formed from buffer alone was also polycrystalline; but it was composed of much smaller individual grains, which had a muted spectrum of colors present (Figure 4*b*). The ices formed from AFP solutions were also composed of smaller grains with muted colors (Figure 4*c*–*e*) and were nearly identical to the ice microstructures present in the buffer alone. These results are consistent with a scenario in which the buffer salts dominate the freezing behavior of AFP solutions, masking any effect that the AFPs themselves might have on the ice microstructure.

Figure 4. Images of frozen droplets taken in cross-polarized light at −16°C: (*a*) water, (*b*) buffer, (*c*) TrxA-*Ap*AFP752, (*d*) cleaved *Ap*AFP752, and (*e*) wild Type III AFP. All solutions were 100 μM. All images taken at the same magnification; scale bar shown in panel *a* is 1 mm.
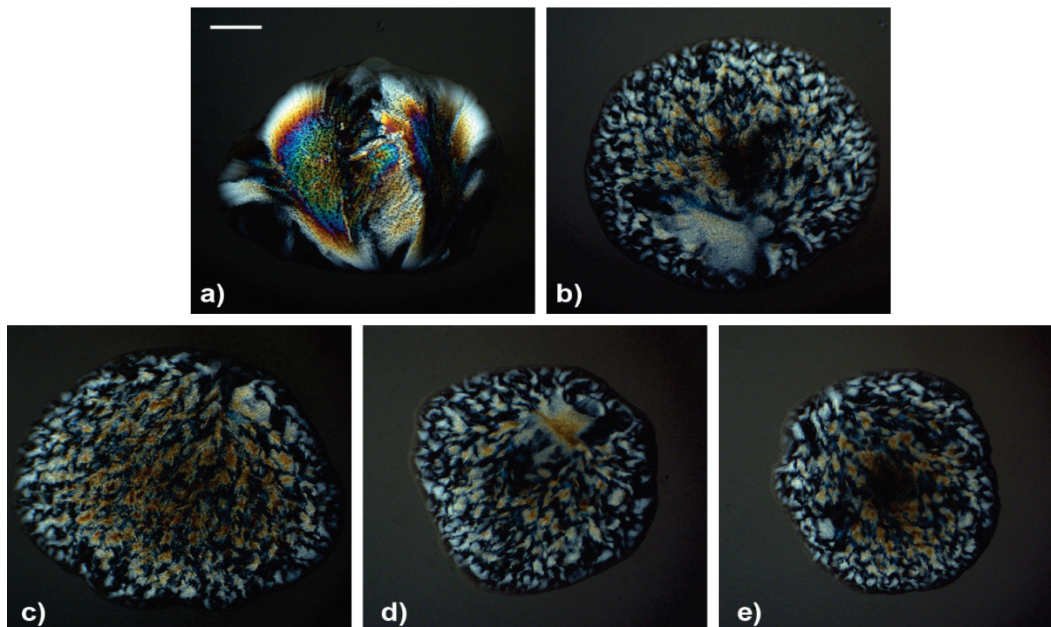
3.2   Splat assay IRI with various AFPs

The IRI for an ice droplet formed from the buffer is shown in Figure 5*a*. After 30 min, the grains already seemed larger because of the Ostwald ripening mechanism. The grains continued to grow larger over the course of 24 hr. In contrast, the TrxA-*Ap*AFP752 and the cleaved *Ap*AFP752, as seen in Figure 5*b* and *c*, respectively, did not show drastic changes in the size of the grains, demonstrating the ability of these compounds to inhibit the recrystallization mechanism. For comparison, the IRI of the Type III AFP is also shown (Figure 5*d*). Over the course of 24 hr, the grains within the ice formed with Type III AFP maintained a similar size, also demonstrating IRI.

Figure 5. Snapshots of the grains of splat assay for sample ice droplets at −8°C over the course of time (0, 0.5, 4, 12, and 24 hr). The samples investigated included the buffer solution (50 mM K_2HP_4, 20 mM NaCl) only, shown in the top row. All AFP solutions (TrxA-*Ap*AFP752, cleaved *Ap*AFP752, and AFP Type III) were at 100 µM concentrations in the same buffer.
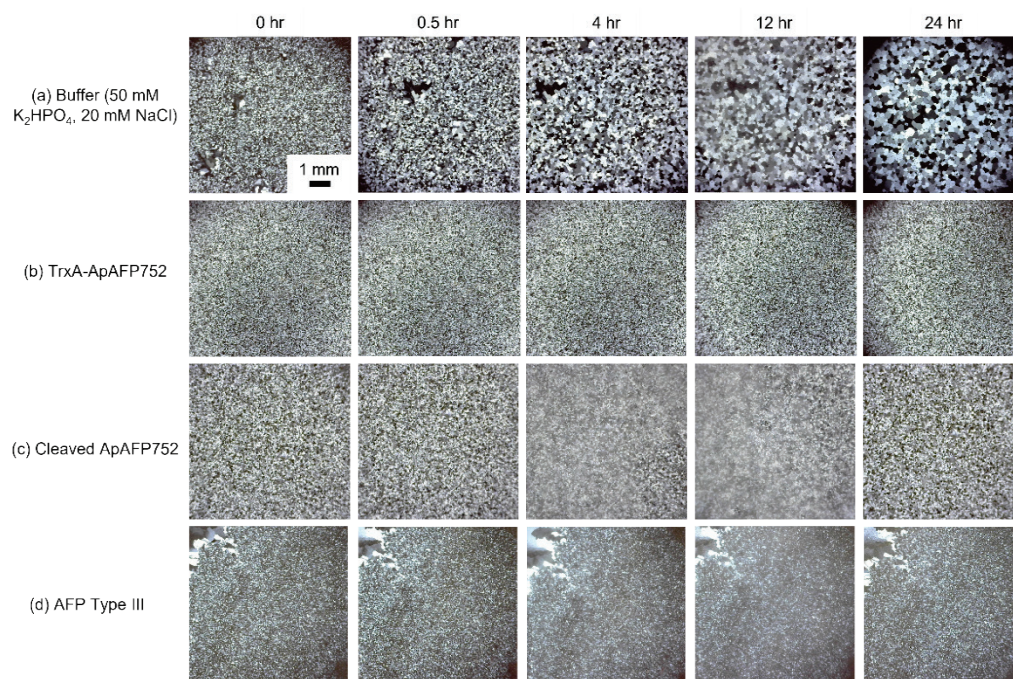
To quantify the IRI results, we analyzed the images from Figure 5 to calculate the MGA. After only 30 min, the IRI abilities of the AFPs were apparent. The MGAs of the Trx-*Ap*AFP752 and the cleaved *Ap*AFP752 were 49.6% and 62.8%, respectively, of that of the buffer. Their average values were within one standard deviation of each other, which means that the IRI ability was unaffected by the cleaving of the fusion protein. The MGA of the Type III AFP was 59.4% of the buffer. This means that all of

these AFPs have similar IRI ability at the same concentration. The MGAs were checked after 24 hr, which is sufficient time to notice a change in grain size and thus to determine if there is IRI activity (Biggs et al. 2019). The MGAs after 24 hr also illustrate that all three AFPs have statistically similar IRI (Figure 6).

Figure 6. Mean grain area (MGA) percentage of each sample compared to the MGA of the buffer after 30 min of annealing at −8°C.
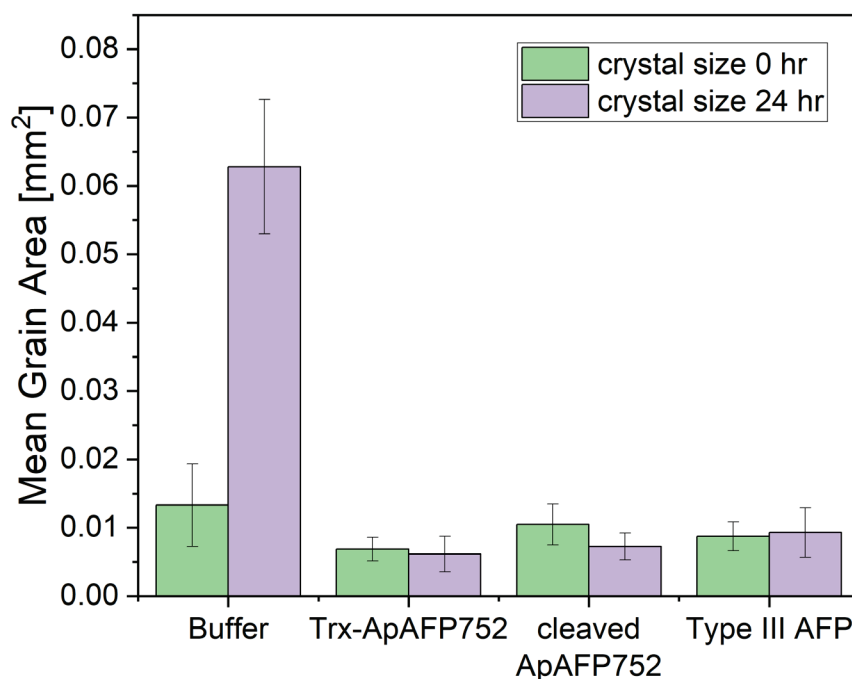
3.3 DIS with various AFPs

We studied the DIS behavior of AFP compounds relative to a buffer solution by growing and monitoring single ice crystals in an optical microscope equipped with a cryo-stage. Figure 7 shows the ice growth of a single ice crystal in a buffer solution, taken in cross-polarized light. The crystal first grew into a hexagonal shape (Figure 7a) and then started to form dendrites, as expected of an ice crystal. Witnessing the ice crystal habit in conjunction with the lack of contrast seen in the optical polarizer implies that the crystal was being viewed along its c-axis, which is the optic axis for the hexagonal ice lattice. A second DIS experiment, shown in Figure 7b, appeared colored in cross-polarized light, indicating that the crystal was not positioned with its c-axis parallel to the view direction. The melting point of the ice crystal formed in buffer solution, found from the temperature just before the ice crystal started growing again, was about −0.30°C. This

was expected based on the calculation of the ideal freezing-point depression of a salt solution:

$$\Delta T_f = K_f \times b \times i,$$

where

ΔT_f = the change in freezing temperature,
K_f = the cryoscopic constant (1.86 K-kg/mol for water),
b = the molality (in moles solute per kilogram solvent), and
i = the van't Hoff factor ($i = 3$ for K_2HPO_4, $i = 2$ for NaCl).

Figure 7. Two different dynamic ice shaping (DIS) experiments for ice crystals growing in a buffer (50 mM K_2HPO_4, 20 mM NaCl) solution with cross-polarized light. Here, (*a*) shows an ice crystal in which the *c*-axis can be assumed to be in the perpendicular direction, while (*b*) shows an ice crystal with the *c*-axis in the parallel direction.
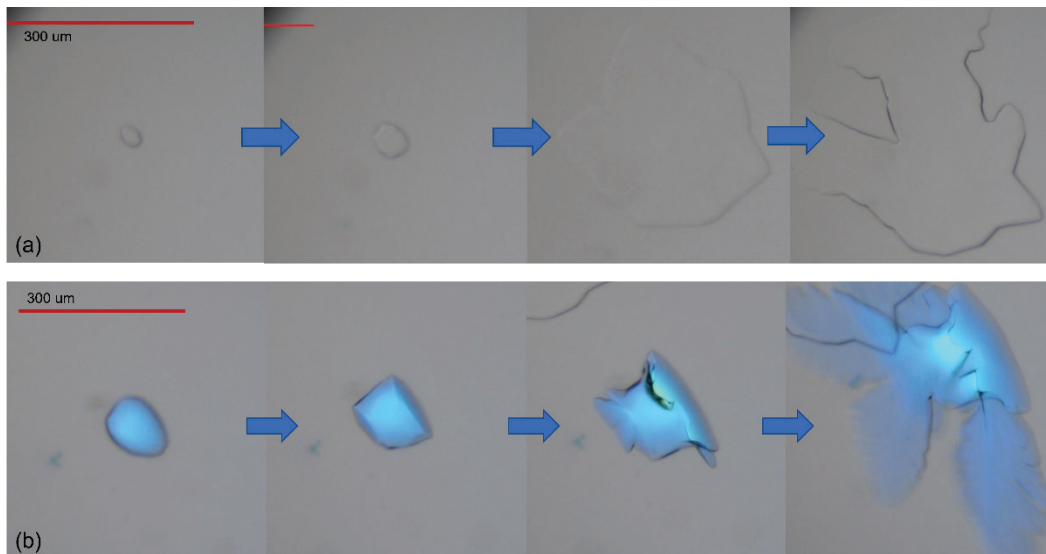
The DIS crystal growth experiment for the TrxA-*Ap*AFP752 is shown in Figure 8*a*. Similar to crystals grown in the buffer, the ice crystal in this AFP solution started to form a hexagonal shape and then continued to grow into dendrites. Notably, a TH was not observed; as soon as the temperature was decreased by even 0.1°C from the melting point to initiate the cooling process, the crystal began to regrow. In other words, we were unable to identify a stability region that is characteristic of a TH. Removing the fusion protein TrxA did not change the ice shaping or delay freezing, as demonstrated in the DIS experiments for the cleaved *Ap*AFP752 in Figure 8*b*. Increasing the concentration of the AFP also did not show any difference regarding the ice growth and TH, as shown in Figure 8*c*.

Figure 8. Microscope images taken at notable changes in shape during DIS experiments for (*a*) 100 µM Trx-*Ap*AFP752, (*b*) 100 µM cleaved *Ap*AFP752, (*c*) 350 µM cleaved *Ap*AFP752 solution, and (*d*) 100 µM Type III AFP solution. Panel *d* was taken in cross-polarized light.
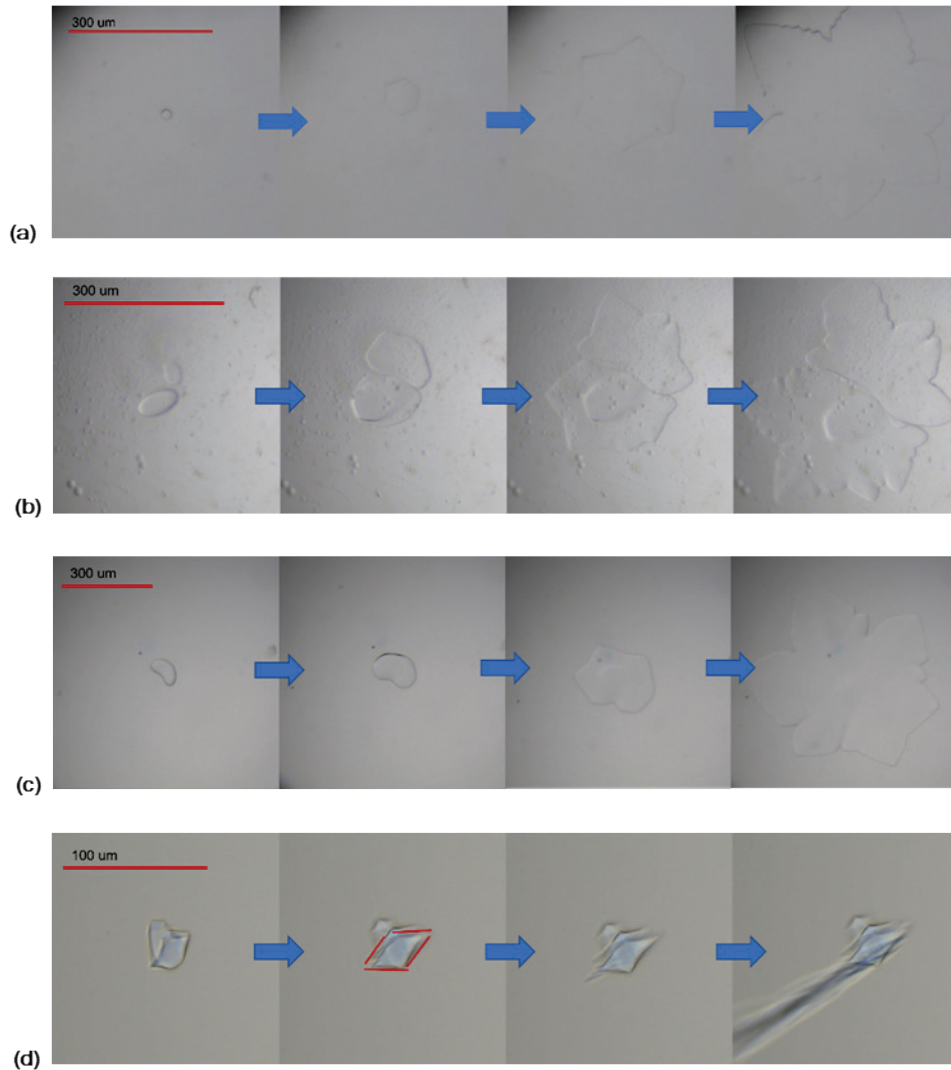
We also studied the ice-shaping behavior of the Type III AFP, shown in Figure 8*d*. For these experiments, it was remarkably easier to follow the reported procedure for studying TH and DIS. Unlike what we observed with the *Ap*AFP752, the crystals with the Type III AFP neither melted nor regrew as the temperature was slightly lowered and held constant for 10 min. For the Type III AFP, the temperature was able to be very slowly lowered, at a rate of 0.1°C/min, compared to the ramp of 1°C/min needed to prevent the *Ap*AFP752 from completely melting. At a certain tempera-ture, the ice crystal changed shape and started growing uniquely; it adopted a diamond shape (highlighted by the red lines in Figure 8*d*) due to the AFP binding to the prism planes, which allowed the crystal to grow

in the *c*-direction instead, as reported in the literature. As the temperature continued to decrease, the ice crystal continued to elongate and "burst" into a needle-like crystal. The TH value was 0.34°C, which is similar to what was reported in the literature (Scotter et al. 2006; Olijve et al. 2016). The noticeable TH and DIS from these AFPs further confirmed that the *Ap*AFP752 sample had no TH or DIS, even at high concentrations.

3.4 Pseudohomogeneous freezing of *Ap*AFP752 solutions

We sought to confirm our findings from the DIS studies, which indicated that *Ap*AFP752 did not have TH. To further understand how AFPs can be leveraged to modulate the freezing behavior of ice, we performed pseudo-homogeneous freezing studies on droplets (10 µL) of AFP solutions suspended in silicone oil. We refer to this experiment as pseudohomogeneous because the droplet was not in contact with a surface but, rather, was suspended in oil and insulated to achieve isothermal conditions in an effort to initiate nucleation within the bulk volume of the droplet.

Figure 9 shows a typical time-versus-temperature profile. During the cooling ramp of each cycle, there is a sharp peak showing a sudden increase in the temperature, which corresponds to the latent heat released during droplet freezing. We defined the freezing temperature for each droplet-freeze cycle as the temperature at the onset of this spike. The average freezing temperature and time for droplets of water, buffer, and different concentrations of *Ap*AFP752 (Figure 10) were all within one standard deviation of each other, showing that *Ap*AFP752 does not affect freezing temperature or time. This is consistent with our observations from DIS studies.

Figure 9. A representative time-versus-temperature profile for droplet-freezing cycles. Data shown were from buffer solution (10 µL droplet).
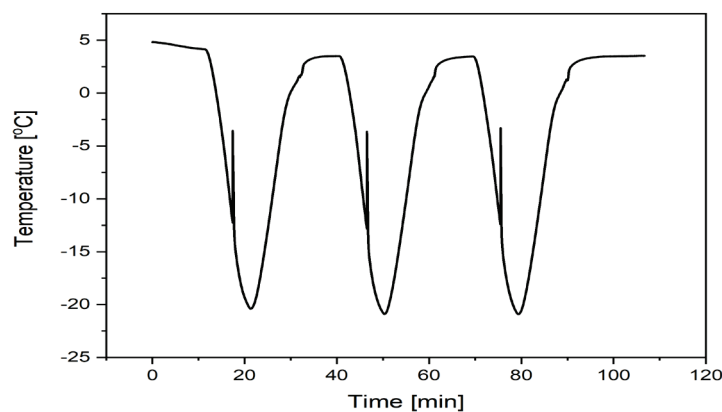
Figure 10. Results from droplet-freezing studies with *Ap*AFP752 solutions under pseudo-homogeneous conditions: (*a*) average freeze temperature and (*b*) average freeze time for variable concentrations of *Ap*AFP752 with reference to buffer and water.

(a)

(b)
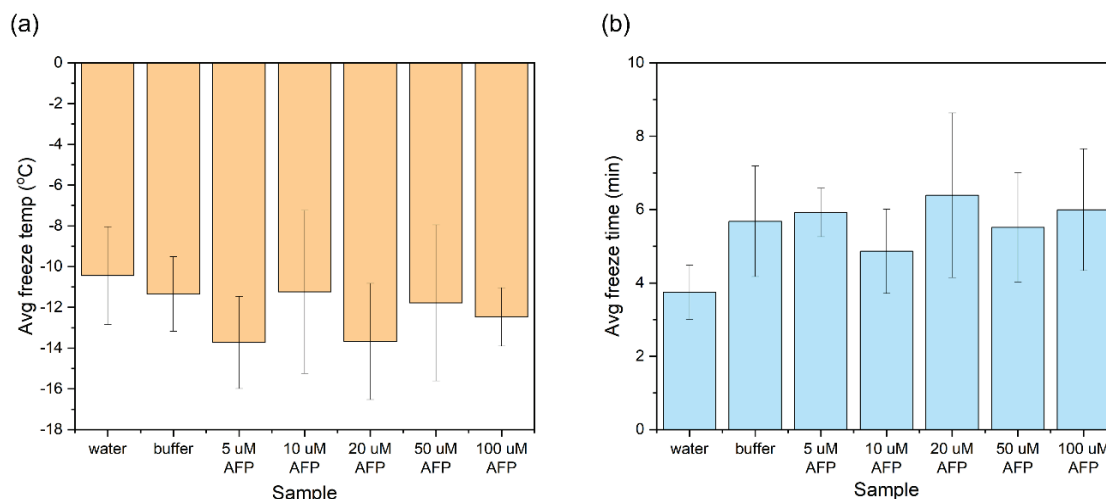
3.5 Heterogeneous freezing of *Ap*AFP752 solutions on clean glass surfaces

To investigate the interaction of *Ap*AFP752 with ice on surfaces, we carried out experiments in which AFP solutions were frozen on clean glass slides. For these experiments, we also monitored droplet freeze temperature as the temperature spiked due to latent heat release, but we used a high-resolution thermal imaging camera. In these images, the latent heat released during the phase transition of water to ice was evidenced by brighter red and yellow regions in the droplet images (Figure 11). By analyzing a circular region of interest (ROI), which was completely encompassed by the droplet, the mean droplet ROI temperature as a function of time was derived. To ensure thermal stability, the temperature profiles for analysis were selected from the second freezing cycle (Figure 12).

Thermal analysis of the water data showed that freezing occurred at −2.4°C, while the buffer solution was observed to freeze at −3.5°C. The *Ap*AFP752 solutions showed a consistent trend of decreasing freezing temperature, from −2.9°C to −3.3°C to −3.6°C, as the concentration was increased from 2.5 to 5.0 to 20 μM; however, with a standard deviation of 0.5°C in the temperature measurements, all the AFP freezing temperatures were statistically equivalent to the buffer. These results corroborate the results from earlier studies (e.g., on droplet microstructure), wherein any potential ice-freezing modulations by *Ap*AFP752 were masked by the colligative effects of the buffer. To fully understand the interactions of

*Ap*AFP752 with ice, the AFP needs to be isolated from the buffer, such as might be accomplished by immobilizing the AFP on a surface.

Figure 11. A representative image of a 10 µL droplet of AFP solution during freezing. *Red* regions are warmer and result from the release of latent heat during solidification of water.
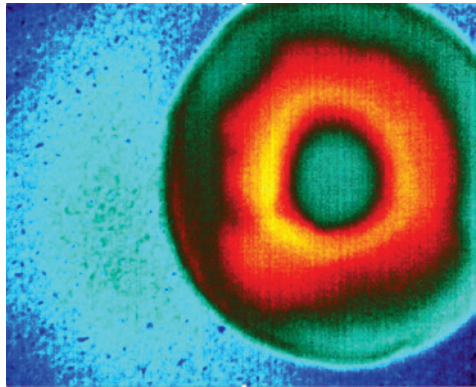
Figure 12. (*a*) A representative plot of the thermal profile imposed to freeze droplets of *Ap*AFP752 solutions on clean glass slides. The freezing events are labeled. (*b*) A focused view of the latent heat released during the second freeze cycle for the *Ap*AFP752 concentrations studied, shown with pure water and the buffer only.
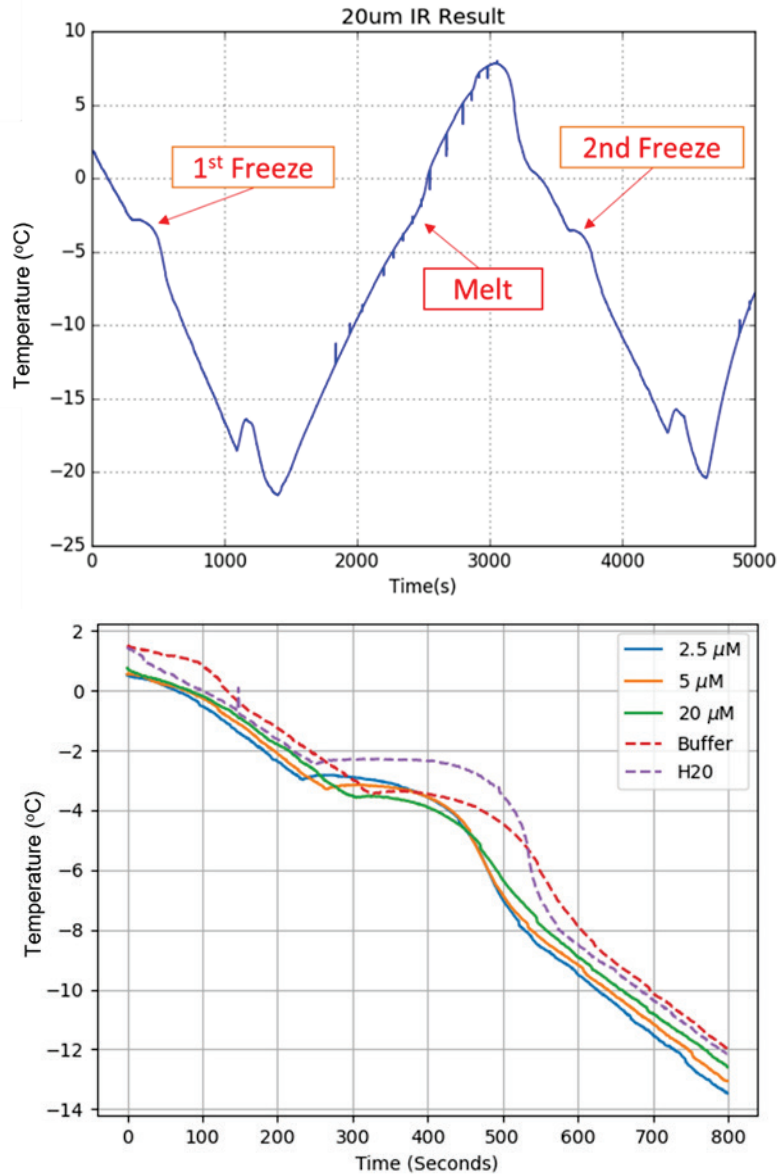
3.6   Surface characterization for *Ap*AFP752-functionalized surfaces

Due to the dominating effects of buffer colligative properties in the freezing studies on *Ap*AFP752, we sought to isolate the AFPs from the buffer by grafting them to glass surfaces. We developed a self-assembly surface chemistry approach that leveraged the pendant thiol present on

*Ap*AFP752. In short, we first added a primary amine to the glass surfaces by silanization with AHAMTES (Figure 13). Next, we carried out a reaction between the primary amine and an N-hydroxysuccinimide (NHS) ester, which was a terminal group in a polyethylene glycol crosslinking agent. With the NHS ester bound to the surface, the new pendant functionality was a maleimide group, which was then reacted with the available thiol on *Ap*AFP752 via Michael Addition. The surface chemistry was tracked at each step by contact angle goniometry, atomic force microscopy (AFM), and FTIR spectroscopy.

Figure 13. Schematic of the experimental procedure to graft *Ap*AFP752 to silica surfaces.

ApAFP752 = anti-freeze protein isolated from *Anatolica polita* beetle
SM(PEG)₂ = succinimidyl-dPEG-maleimide

AHAMTES = aminohexyl aminomethyl triethoxysilane
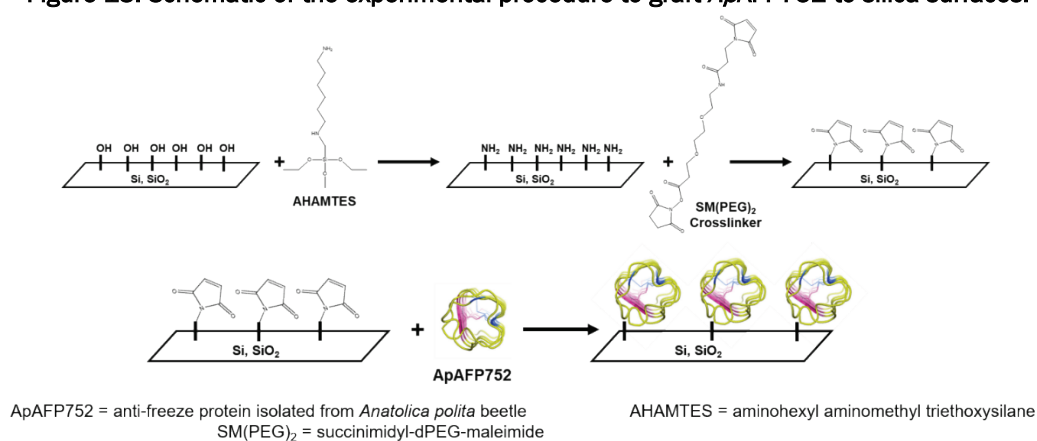
We measured an increase in the contact angle of the amine-terminated surface over a freshly cleaned (i.e., pristine) glass slide, as expected based on the reduction in hydroxyl groups (Asenath-Smith and Chen 2008). A subsequent decrease in contact angle was expected after grafting with the crosslinker SM(PEG)$_2$ due to the increase in oxygen-containing functionalities. We observed both relative changes in contact angle (Figure 14). To further confirm the successful reaction of the crosslinker with the surface, we used high-performance chromatography to monitor the decrease of crosslinker from the solution and found a decrease of over 80% in 2 hr (results not shown). These results indirectly indicated that the crosslinker was tethered to the surface.

Figure 14. Dynamic contact angle measurements of AFP-functionalized surfaces and control surfaces. All bars and points represent the average of five values, and error bars are the standard deviation of five values. All tests were conducted with 10 μL drops of Milli-Q water, except for those on the Piranha-cleaned slides, where 5 μL drops were used.
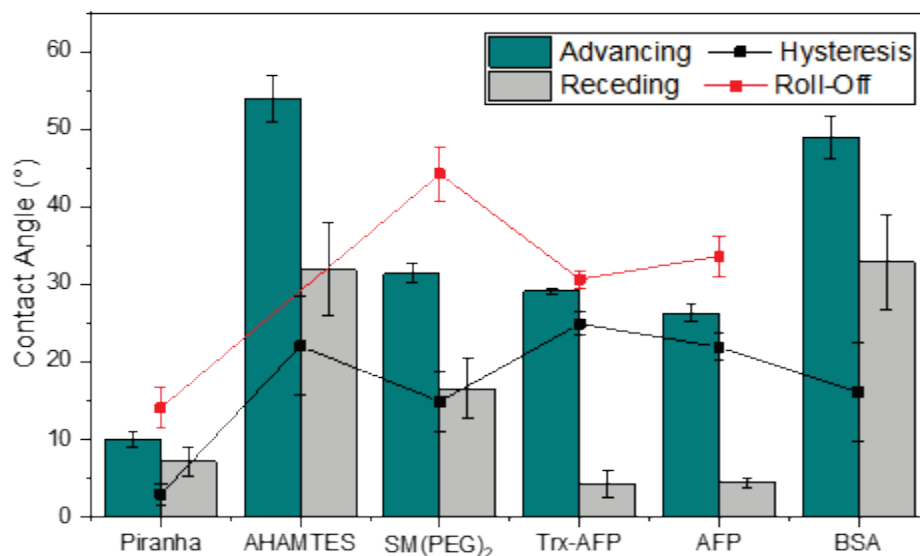
We only observed a minimal change in contact angle after reaction with the TrxA-AFP752 and *Ap*AFP752 to the maleimide, which was unexpected due to the relative abundance of hydrophobic components present in proteins. This observation raised the question of whether the AFPs were on the surface. To further investigate for the changes in bonding and chemical groups on the surface, we attempted characterization with FTIR using variable angle grazing incidence techniques, but the results were inconclusive due to low detector sensitivity (results not shown).

As a control experiment to our protein grafting, we carried out the same sequence of reactions but used BSA in place of the AFP. The BSA protein has an available thiol, so this experiment was chosen to confirm that our surface chemistry process was proceeding as designed and to disaggregate any issues that may have been specific to the AFPs themselves. After reacting BSA with the crosslinker surface, the contact angle increased to $48 \pm 3°$, consistent with the presence of a hydrophobic protein on the surface.

We further studied the surface modifications with AFM, looking for changes in roughness at each functionalization step (Figure 15). After reaction with AHAMTES, the roughness of the surface increased from Ra = 0.429 nm to 0.658 nm, consistent with the presence of a thin monolayer. After grafting the SM(PEG)₂ crosslinker, we observed the roughness to

decrease rather than increase as expected. In fact, the Ra value of 0.424 nm was on par with that of the pristinely clean glass slide (Figure 15a), yet the chromatography studies mentioned previously strongly indicated that the crosslinker was deposited on the surface. In these studies, we used the short chain crosslinker, $n = 2$, so changes in roughness are not sufficient to draw firm conclusions about the presence of the molecular species on the surface. We also observed no change in surface roughness after reaction with the AFPs, a result which was unexpected given the bulky nature of proteins. Meanwhile, the AFM images of the BSA control surface revealed distinct islands of high intensity, and the roughness increased significantly to Ra = 1.47 nm. These results draw into question the availability of the thiol group on TrxA-ApAFP752 and ApAFP752, which is needed to react the AFPs with the maleimide on the surface.

Figure 15. Atomic force microscopy (AFM) scans of glass substrates (a) cleaned with Piranha and functionalized with (b) AHAMTES, (c) SM(PEG)₂ crosslinker, (d) ApAFP752, and (e) BSA control protein. Mean roughness values (Ra) for each scan are shown on each image.
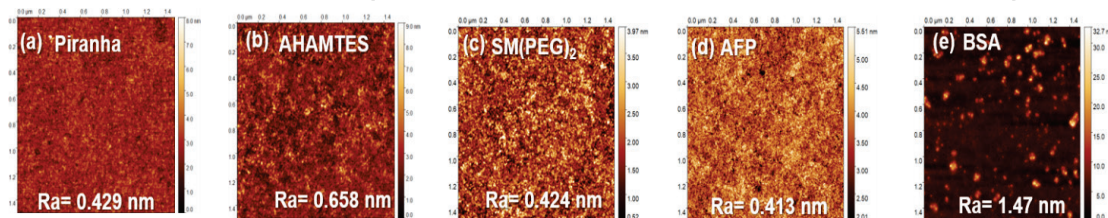
To look for an available thiol in the ApAFP752 protein, we conducted FTIR studies on concentrated micromolar solutions, using water as a reference (Figure 16). Despite the ApAFP752 spectrum being mostly dominated by the water, the C-O peak from the threonine residue was still noticeable at 1,075 cm⁻¹. However, the characteristic thiol peak at 2,550 cm⁻¹ from the cysteine residue could not be seen, and the spectrum for ApAFP752 was flat in that key region. These results further indicated that the thiol group needed for surface reactions with maleimide was not available.

Figure 16. Fourier transform infrared (FTIR) spectra of a highly concentrated
*Ap*AFP752 solution (*blue*), compared to that of pure water (*black*).
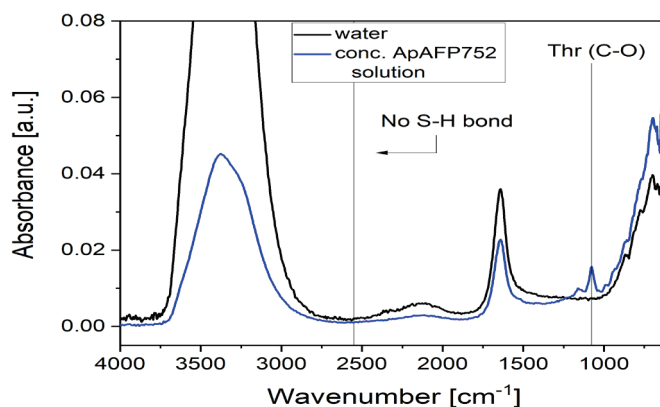
3.7 Heterogeneous freezing of water on functionalized surfaces

Despite inconclusive results from surface characterization and chemical analysis about whether the AFPs were present on the surface, we carried out some droplet-freezing studies. In these studies, we froze pure water droplets (10 µL) on glass slides with variable surface chemistries. In short, after the deposition of water on the target surface, the droplet was sealed with another glass slide and subject to a temperature ramp while the temperature was monitored at the droplet (Figure 17). The onset of freezing was determined from the temperature rise caused by the latent heat of freezing (Figure 17 inset).

Figure 17. Temperature profiles during the freezing experiments. The probes are labeled as follows: *Air in Chamber* was the inside wall of the large environmental chamber, *Air in Box* refers to the smaller enclosure that housed the experimental apparatus, *Sample* temperature was taken on the glass slide directly under the droplet, and *Stage* temperature was taken on the metal stage adjacent to the mounted sample. *Inset*: the thermal trace from *Sample* shows the increase of temperature induced by the freezing of the droplet.
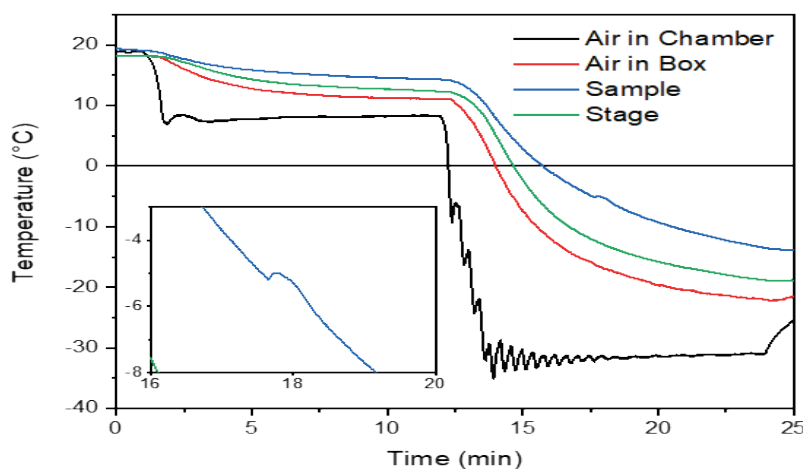
In addition to temperature data, droplet freezing was manifest in the microscope images taken during these studies. With these images (Figure 18), we were able to assign an approximate nucleation time as the time when a contrast change was first observed in the droplet (time 11:49, Figure 18). Statistical results on the average freeze time and average nucleation time are summarized in Figure 19. No significant difference was seen between the average freezing times or nucleation temperatures of water droplets on different surfaces.

Figure 18. A representative series of time-lapse images for a water droplet freezing on a chemically modified substrate. This figure shows the freezing of a water droplet on a surface that had been reacted with *Ap*AFP752.
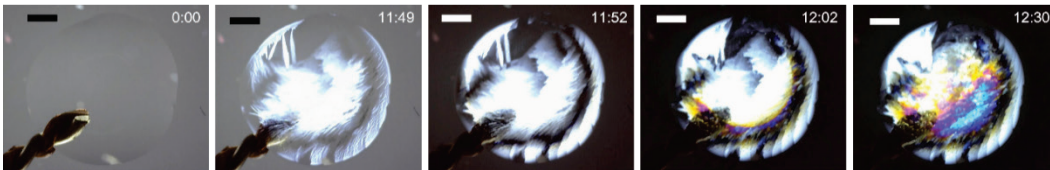
Figure 19. Results from droplet freezing on chemically modified substrates: (*a*) average freezing temperature taken from the start of the peak in the thermal data and (*b*) average nucleation start time for each sample taken as the time when ice crystals were first seen in the microscope images.
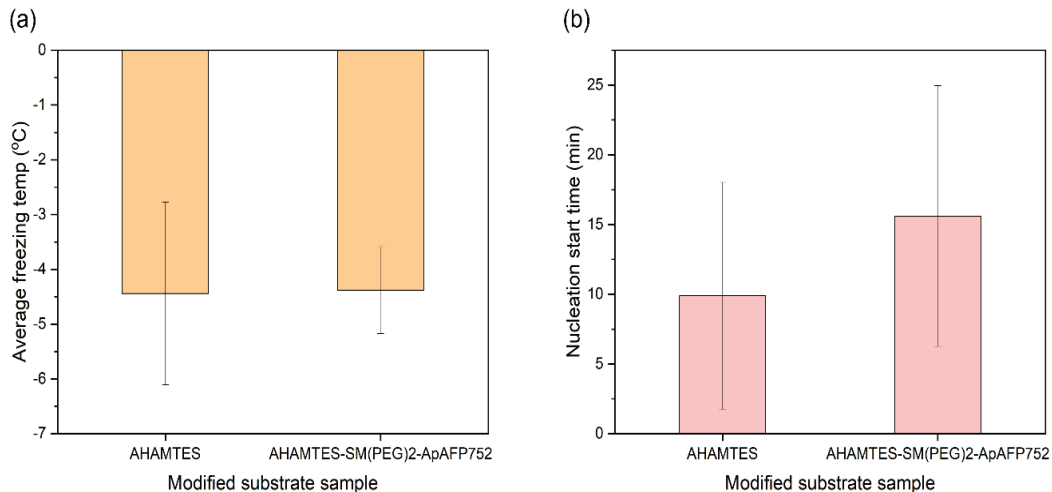
4 Discussion

The results presented herein demonstrated that *Ap*AFP752 has very little effect on the freezing of ice: the microstructure of polycrystalline ice and both the pseudohomogeneous and heterogeneous freezing temperatures were all statistically similar to those of the buffer alone. Attempts to study *Ap*AFP752 by tethering it to a surface were unsuccessful, possibly due to a lack of availability of the necessary thiol group. It is noteworthy, however, that while *Ap*AFP752 did not show any effect on freezing temperature or microstructure, it did have the ability to inhibit IRI.

The lack of DIS and TH of *Ap*AFP752 observed during our experiments is consistent with the null effects on freezing discussed above. These results are especially puzzling because previous studies have demonstrated that *Ap*AFP752 has a TH (Mao et al. 2010). Observing a TH and DIS is expected for the *Ap*AFP752 because it shares characteristics (i.e., the TCT sequence and the beta-helix structure) with hyperactive AFPs. However, the *Ap*AFP752 we tested through these experiments did not show any significant change in freezing temperature or DIS. Interestingly, despite the lack of TH and DIS, *Ap*AFP752 still showed IRI activity, which is perplexing as it has been hypothesized that ice binding also affects IRI activity (Rahman et al. 2019).

It is also possible that an AFP can exhibit IRI activity but not necessarily show any TH or DIS. Some studies have suggested that there is no mechanistic relationship between the TH, DIS, and IRI activity (Gruneberg et al. 2021). It is possible that one of the mechanisms for IRI may not even depend on any ice binding; one hypothesis was that the AFP can prevent ice recrystallization staying within the quasi-liquid layer of the forming ice, instead of actually binding to the ice (Biggs et al. 2019). However, the reasons for this lack of correlation between TH and IRI are still not entirely understood.

One possible explanation for this discrepancy in results is that the protein has undergone unfolding. An extra cysteine was added to *Ap*AFP752 to facilitate subsequent derivatizations with other chemical moieties. This cysteine or different expression conditions could have disturbed the cysteine residues in the disulfide linkages that formed the beta-helix structure, causing the protein to unfold (De Rosa et al. 2021). Because DIS and TH are highly dependent on the ice-binding site maintained from the

structure of the AFP, an unfolded protein would result in a loss of activity, and thus, there would be no DIS or TH. Characterization of the AFP structure would be needed to fully confirm that this is the case.

The FTIR analysis on a highly concentrated ApAFP752 solution showed no peak corresponding to the presence of S-H bonds. This could explain why the ApAFP752 was not detected on the glass surfaces after undergoing functionalization; the S-H bond is crucial to reacting with the maleimide functional group of the $SM(PEG)_n$ crosslinker (Thermo Scientific 2012).

Whether DIS, TH, or IRI is a more important antifreeze property for controlling icing depends on the application. For instance, in the field of cryopreservation, having a high IRI and a low TH is desirable because ice shaping and ice regrowth can cause damage to the cells or organs being preserved (Chang and Zhao 2021). From our results, it seems that the AFP having no DIS or TH correlates to the lack of change in freezing droplets. However, it is still unclear which AFP properties are associated with reduced ice adhesion.

5   Conclusions

Results from various freezing experiments showed that neither the TrxA-*Ap*AFP752 nor cleaved *Ap*AFP752 showed any significant difference in shaping ice during growth or delaying or preventing freezing. These observations were supported by the noticeable DIS and TH exhibited by the Type III AFP. As a result of the lack of activity from *Ap*AFP752, freezing experiments for *Ap*AFP752 appeared to be dominated by the colligative effects of the buffer solution instead of by the AFP itself. However, *Ap*AFP752 exhibited IRI activity, suggesting that the mechanisms for IRI, TH, and DIS for AFPs are not necessarily related. In addition, attempts to graft *Ap*AFP752 to glass surfaces for further freezing studies left open questions about the availability of the needed thiol group on the AFP for reaction with the pendant maleimide on the surface. Additional studies on the presence and location of the thiol group are needed before further surface grafting studies can proceed.

References

Asenath-Smith, E., and W. Chen. 2008. "How to Prevent the Loss of Surface Functionality Derived from Aminosilanes." *Langmuir* 24 (21): 12405–12409. https://doi.org/10.1021/la802234x.

Bialkowska, A., E. Majewska, A. Olczak, and A. Twarda-Clapa. 2020. "Ice Binding Proteins: Diverse Biological Roles and Applications in Different Types of Industry." *Biomolecules* 10 (2): 274. https://doi.org/10.3390/biom10020274.

Biggs, C. I., C. Stubbs, B. Graham, A. E. R. Fayter, M. Hasan, and M. I. Gibson. 2019. "Mimicking the Ice Recrystallization Activity of Biological Antifreezes. When Is a New Polymer 'Active'?" *Macromolecular Bioscience* 19 (7): e1900082. https://doi.org/10.1002/mabi.201900082.

Budke, C., C. Heggemann, M. Koch, N. Sewald, and T. Koop. 2009. "Ice Recrystallization Kinetics in the Presence of Synthetic Antifreeze Glycoprotein Analogues Using the Framework of LSW Theory." *Journal of Physical Chemistry B* 113 (9): 2865–2873. https://doi.org/10.1021/jp805726e.

Budke, C., and T. Koop. 2006. "Ice Recrystallization Inhibition and Molecular Recognition of Ice Faces by Poly(Vinyl Alcohol)." *ChemPhysChem* 7 (12): 2601–2606. https://doi.org/10.1002/cphc.200600533.

Cao, Y. H., W. Y. Tan, and Z. L. Wu. 2018. "Aircraft Icing: An Ongoing Threat to Aviation Safety." *Aerospace Science and Technology* 75 (April): 353–385. https://doi.org/10.1016/j.ast.2017.12.028.

Celik, Y., L. A. Graham, Y.-F. Mok, M. Bar, P. L. Davies, and I. Braslavsky. 2010. "Superheating of Ice Crystals in Antifreeze Protein Solutions." *PNAS* 107 (12): 5423–5428. https://doi.org/10.1073/pnas.0909456107.

Chakraborty, S., and B. Jana. 2019. "Ordered Hydration Layer Mediated Ice Adsorption of a Globular Antifreeze Protein: Mechanistic Insight." *Physical Chemistry Chemical Physics* 21 (35): 19298–19310. https://doi.org/10.1039/c9cp03135a.

Chang, T., and G. Zhao. 2021. "Ice Inhibition for Cryopreservation: Materials, Strategies, and Challenges." *Advanced Science* 8 (6): 2002425. https://doi.org/10.1002/advs.202002425.

Chao, H., F. D. Sönnichsen, C. I. DeLuca, B. D. Sykes, and P. L. Davies. 1994. "Structure-Function Relationship in the Globular Type-III Antifreeze Protein: Identification of a Cluster of Surface Residues Required for Binding to Ice." *Protein Science* 3 (10): 1760–1769. https://doi.org/10.1002/pro.5560031016.

Clarke, C. J., S. L. Buckley, and N. Lindner. 2002. "Ice Structuring Proteins—A New Name for Antifreeze Proteins." *Cryo Letters* 23 (2): 89–92.

De Rosa, L., R. Di Stasi, A. Romanelli, and L. D. D'Andrea. 2021. "Exploiting Protein N-Terminus for Site-Specific Bioconjugation." *Molecules* 26 (12): 3521. https://doi.org/10.3390/molecules26123521.

Drori, R., Y. Celik, P. L. Davies, and I. Braslavsky. 2014. "Ice-Binding Proteins That Accumulate on Different Ice Crystal Planes Produce Distinct Thermal Hysteresis Dynamics." *Journal of the Royal Society Interface* 11 (98): 20140526. https://doi.org/10.1098/rsif.2014.0526.

Esser-Kahn, A. P., V. Trang, and M. B. Francis. 2010. "Incorporation of Antifreeze Proteins into Polymer Coatings Using Site-Selective Bioconjugation." *Journal of the American Chemical Society* 132 (38): 13264–13269. https://doi.org/10.1021/ja103038p.

Garnham, C. P., R. L. Campbell, and P. L. Davies. 2011. "Anchored Clathrate Waters Bind Antifreeze Proteins to Ice." *Proceedings of the National Academy of Sciences of the United States of America* 108 (18): 7363–7367. https://doi.org/10.1073/pnas.1100429108.

Gerhauser, J., and V. Gaukel. 2021. "Detailed Analysis of the Ice Surface after Binding of an Insect Antifreeze Protein and Correlation with the Gibbs–Thomson Equation." *Langmuir* 37 (40): 11716–11725.

Ghalamara, S., S. Silva, C. Brazinha, and M. Pintado. "Structural Diversity of Marine Anti-Freezing Proteins, Properties and Potential Applications: A Review." *Bioresources and Bioprocessing* 9 (5): 1–24. https://doi.org/10.1186/s40643-022-00494-7.

Graether, S. P., M. J. Kuiper, S. M. Gagné, V. K. Walker, Z. C. Jia, B. D. Sykes, and P. L. Davies. 2000. "β-Helix Structure and Ice-Binding Properties of a Hyperactive Antifreeze Protein from an Insect." *Nature* 406 (July): 325–328. https://doi.org/10.1038/35018610.

Gruneberg, A. K., L. A. Graham, R. Eves, P. Agrawal, R. D. Oleschuk, and P. L. Davies. 2021. "Ice Recrystallization Inhibition Activity Varies with Ice-Binding Protein Type and Does Not Correlate with Thermal Hysteresis." *Cryobiology* 99 (April): 28–39. https://doi.org/10.1016/j.cryobiol.2021.01.017.

Gwak, Y., J. I. Park, M. Kim, H. S. Kim, M. J. Kwon, S. J. Oh, Y. P. Kim, and E. Jin. 2015. "Creating Anti-icing Surfaces via the Direct Immobilization of Antifreeze Proteins on Aluminum." *Scientific Reports* 5: 12019. https://doi.org/10.1038/srep12019.

Hori, M., T. Aoki, T. Tanikawa, A. Hachikubo, K. Sugiura, K. Kuchiki, and M. Niwano. "Modeling Angular-Dependent Spectral Emissivity of Snow and Ice in the Thermal Infrared Atmospheric Window." *Applied Optics* 52 (30): 7243–7255.

Knight, C. A., J. Hallett, and A. L. Devries. 1988. "Solute Effects on Ice Recrystallization: An Assessment Technique." *Cryobiology* 25 (1): 55–60. https://doi.org/10.1016/0011-2240(88)90020-X.

Koshio, K., K. Arai, T. Waku, P. W. Wilson, and Y. Hagiwara. 2018. "Suppression of Droplets Freezing on Glass Surfaces on Which Antifreeze Polypeptides Are Adhered by a Silane Coupling Agent." *PLoS One* 13 (10): e0204686. https://doi.org/10.1371/journal.pone.0204686.

Liou, Y.-C., A. Tocilj, P. L. Davies, and Z. C. Jia. 2000. "Mimicry of Ice Structure by Surface Hydroxyls and Water of a β-Helix Antifreeze Protein." *Nature* 406: 322–324. https://doi.org/10.1038/35018604.

Liu, K., C. Wang, J. Ma, G. Shi, X. Yao, H. Fang, Y. Song, and J. Wang. 2016. "Janus Effect of Antifreeze Proteins on Ice Nucleation." *Proceedings of the National Academy of Sciences of the United States of America* 113 (51): 14739–14744. https://doi.org/10.1073/pnas.1614379114.

Mao, X., Z. Liu, H. Li, J. Ma, and F. Zhang. 2010. "Calorimetric Studies on an Insect Antifreeze Protein ApAFP752 from *Anatolica polita*." *Journal of Thermal Analysis and Calorimetry* 104 (1): 343–349. https://doi.org/10.1007/s10973-010-1067-3.

Mao, X., Z. Liu, J. Ma, H. Pang, and F. Zhang. 2011. "Characterization of a Novel β-Helix Antifreeze Protein from the Desert Beetle *Anatolica polita*." *Cryobiology* 62 (2): 91–99. https://doi.org/10.1016/j.cryobiol.2011.01.001.

Olijve, L. L. C., K. Meister, A. L. DeVries, J. G. Duman, S. Guo, H. J. Bakker, and I. K. Voets. 2016. "Blocking Rapid Ice Crystal Growth through Nonbasal Plane Adsorption of Antifreeze Proteins." *Proceedings of the National Academy of Sciences of the United States of America* 113 (14): 3740–3745. https://doi.org/10.1073/pnas.1524109113.

Rahman, A. T., T. Arai, A. Yamauchi, A. Miura, H. Kondo, Y. Ohyama, and S. Tsuda. 2019. "Ice Recrystallization Is Strongly Inhibited When Antifreeze Proteins Bind to Multiple Ice Planes." *Scientific Reports* 9 (1): 2212. https://doi.org/10.1038/s41598-018-36546-2.

Scotter, A. J., C. B. Marshall, L. A. Graham, J. A. Gilbert, C. P. Garnham, and P. L. Davies. 2006. "The Basis for Hyperactivity of Antifreeze Proteins." *Cryobiology* 53 (2): 229–239. https://doi.org/10.1016/j.cryobiol.2006.06.006.

Takamichi, M., Y. Nishimiya, A. Miura, and S. Tsuda. 2009. "Fully Active QAE Isoform Confers Thermal Hysteresis Activity on a Defective SP Isoform of Type III Antifreeze Protein." *FEBS Journal* 276 (5): 1471–1479. https://doi.org/10.1111/j.1742-4658.2009.06887.x.

Thermo Scientific. 2012. *Thermo Scientific Crosslinking Technical Handbook*. Waltham, MA: Thermo Scientific. https://tools.thermofisher.com/content/sfs/brochures/1602163-Crosslinking-Reagents-Handbook.pdf.

Verreault, D., S. Alamdari, S. J. Roeters, R. Pandey, J. Pfaendtner, and T. Weidner. 2018. "Ice-Binding Site of Surface-Bound Type III Antifreeze Protein Partially Decoupled from Water." *Physical Chemistry Chemical Physics* 20 (42): 26926–26933. https://doi.org/10.1039/c8cp03382j.

Abbreviations

AFP	Antifreeze protein
AFM	Atomic force microscopy
AHAMTES	N-(6-aminohexyl)aminomethyltriethoxysilane
BSA	Bovine serum albumin
DIS	Dynamic ice shaping
DMSO	Dimethyl sulfoxide
DTGS	Deuterated triglycine sulfate
EDTA	Ethylenediaminetetraacetic acid
FTIR	Fourier Transform Infrared
IBS	Ice-binding surface
IR	Infrared
IRI	Ice recrystallization inhibition
MGA	Mean grain area
NHS	N-hydroxysuccinimide
PBS	Phosphate-buffered saline
QAE	Quaternary aminoethyl
Ra	Roughness value
ROI	Region of interest
SP	Sulfopropyl
T	Threonine
TCT	Threonine-cysteine-threonine
TH	Thermal hysteresis

X   Amino acid

REPORT DOCUMENTATION PAGE

Form Approved
OMB No. 0704-0188

1. REPORT DATE (DD-MM-YYYY)	2. REPORT TYPE	3. DATES COVERED (From - To)
September 2022	Final	FY18–FY22

4. TITLE AND SUBTITLE	5a. CONTRACT NUMBER
Investigations into the Ice Crystallization and Freezing Properties of the Antifreeze Protein *Ap*AFP752	
	5b. GRANT NUMBER
	5c. PROGRAM ELEMENT

6. AUTHOR(S)	5d. PROJECT NUMBER
Emily Asenath-Smith, Emily C. Jeng, Emma K. Ambrogi, Garrett R. Hoch, and Jason L. Olivier	611102AH68
	5e. TASK NUMBER
	5f. WORK UNIT NUMBER

7. PERFORMING ORGANIZATION NAME(S) AND ADDRESS(ES)	8. PERFORMING ORGANIZATION REPORT NUMBER
US Army Engineer Research and Development Center (ERDC) Cold Regions Research and Engineering Laboratory (CRREL) 72 Lyme Road Hanover, NH 03755-1290	ERDC/CRREL TR-22-17

9. SPONSORING / MONITORING AGENCY NAME(S) AND ADDRESS(ES)	10. SPONSOR/MONITOR'S ACRONYM(S)
National Aeronautics and Space Administration Goddard Space Flight Center Headquarters Procurement Office Greenbelt, MD 20771	NASA
	11. SPONSOR/MONITOR'S REPORT NUMBER(S)

12. DISTRIBUTION / AVAILABILITY STATEMENT
Approved for public release; distribution is unlimited.

13. SUPPLEMENTARY NOTES
This study was conducted for the National Aeronautics and Space Administration (NASA) under the Established Program to Stimulate Competitive Research (EPSCoR) program (Award No. 80NSSC18M0034), "Application of Antifreeze Proteins and Mimetic Peptides in Anti-Icing Surface Coating." MIPR 80HQTR18T0062

14. ABSTRACT

Antifreeze proteins (AFPs) allow biological organisms, including insects, fish, and plants, to survive in freezing temperatures. While in solution, AFPs impart cryoprotection by creating a thermal hysteresis (TH), imparting ice recrystallization inhibition (IRI), and providing dynamic ice shaping (DIS). To leverage these ice-modulating effects of AFPs in other scenarios, a range of icing *assays* were performed with AFPs to investigate how AFPs interact with ice formation when tethered to a surface.

In this work, we studied *Ap*AFP752, an AFP from the beetle *Anatolica polita*, and first investigated whether removing the fusion protein attached during protein expression would result in a difference in freezing behavior. We performed optical microscopy to examine ice-crystal shape, microstructure, and recrystallization behavior of frozen droplets of AFP solutions. We developed a surface chemistry approach to tether these proteins to glass surfaces and conducted droplet-freezing experiments to probe the interactions of these proteins with ice formed on those surfaces.

In solution, *Ap*AFP752 did not show any DIS or TH, but it did show IRI capabilities. In surface studies, the freezing of AFP droplets on clean glass surfaces showed no dependence on concentration, and the results from freezing water droplets on AFP-decorated surfaces were inconclusive.

15. SUBJECT TERMS
Antifreeze protein; Cryoprotection; Crystallization; Ice materials; Ice mechanics; Ice prevention and control; Ice recrystallization; Interfaces; Self-assembly; Surface chemistry

16. SECURITY CLASSIFICATION OF:			17. LIMITATION OF ABSTRACT	18. NUMBER OF PAGES	19a. NAME OF RESPONSIBLE PERSON
a. REPORT	b. ABSTRACT	c. THIS PAGE	SAR	42	19b. TELEPHONE NUMBER (include area code)
Unclassified	Unclassified	Unclassified			